Journal of Catalysis **209,** 25–34 (2002)
doi:10.1006/jcat.2002.3588

Surface Properties and Physicochemical Characterizations of a New Type of Anode Material, $La_{1-x}Sr_xCr_{1-y}Ru_yO_{3-\delta}$, for a Solid Oxide Fuel Cell under Methane at Intermediate Temperature

A.-L. Sauvet,*[,1] J. Fouletier,* F. Gaillard,† and M. Primet†

*Laboratoire d'Electrochimie et de Physico-Chimie des Matériaux et des Interfaces INPG, UJF et CNRS, 1130, rue de la piscine-Domaine Universitaire, 38402 Saint Martin d'Hères Cedex, France; and †Laboratoire d'Application de la Chimie à l'Environnement (LACE), UMR, CNRS 5634, Université Claude Bernard, 43 Bd du 11 novembre 1918, 69 622 Villeurbanne Cedex, France

Received August 13, 2001; revised January 21, 2002; accepted February 18, 2002

In order to develop a new anodic material for a solid oxide fuel cell (SOFC) operated under methane, we studied lanthanum chromites doped with strontium and ruthenium. Ruthenium is an excellent catalyst for methane steam reforming but its use is limited by its cost and evaporation as RuO_x at high temperature. To stabilize the ruthenium, we inserted it into the perovskite to form $La_{1-x}Sr_xCr_{1-y}Ru_yO_3$. XRD, SEM, TPR, and EDX analyses revealed the stability of ruthenium in the perovskite, in the tetravalent state. The composition was homogeneous in the entire volume of the electrode. Nevertheless, XPS analyses indicated a strontium segregation for a thickness lower than 5 nm. The EDX analyses also showed a strontium concentration gradient near the subsurface. The main result was that no loss of ruthenium was detected even after treatments under air at 1100°C. The strontium doping allows the stabilization of the ruthenium in the perovskite in the tetravalent state.

Key Words: **perovskite; ruthenium; XPS; TPR; methane reforming; catalytic activity.**

1. INTRODUCTION

One of the significant advantages of a high-temperature solid oxide fuel cell (SOFC) is its ability to operate on fuels such as natural gas or biogas. Conversion of methane can be carried out along different process routes, i.e., external or internal reforming (1). In the first case, the reforming reaction takes place in a separate reforming reactor, a package of outside fired tubes filled with nickel or noble metal catalysts. For high methane conversion and to avoid carbon deposition, steam has to be supplied by exceeding the stoichiometry of the steam reforming reaction. The cost and the volume of the reactor limit this process. Moreover the flexibility of the SOFC's response to load change is hindered by the inertia of the reformer. Internal reforming should be a more attractive solution. However, its development is hindered by carbon deposition and by the endothermicity of this reaction, which produces local cooling in the cell. An alternative process, called gradual internal steam reforming, has been proposed (2). This concept is based on a coupling between the steam reforming reaction (Eq. 1) and the electrochemical hydrogen oxidation (Eq. 2). This allows the reaction to be delocalized over the entire electrode surface and the steam content to be reduced since water produced by hydrogen oxidation is used to convert methane.

$$CH_4 + H_2O \leftrightarrows 3H_2 + CO \quad [1]$$

$$H_2 + O^{2-} \leftrightarrows H_2O + 2e^- \quad [2]$$

Conversion of CO can proceed either via electrochemical oxidation (Eq. 3),

$$CO + O^{2-} \leftrightarrows CO_2 + 2e^-, \quad [3]$$

or by the water–gas shift reaction,

$$CO + H_2O \leftrightarrows CO_2 + H_2, \quad [4]$$

followed by reaction (Eq. 2).

The cermet Ni–YSZ is the commonly used anode. Indeed, nickel is an excellent catalyst for methane reforming and for electrochemical hydrogen oxidation. However, at this time, employment of this anode is limited due to several problems, for example carbon deposition, which deactivates the catalyst. Thus, dilution of natural gas is necessary.

Lanthanum chromites have been intensively studied as promising interconnects for SOFC. The perovskite phase is stable at high temperature (1000°C) and across a wide P_{O2} range (1–10^{-20} bar) (3). Pure $LaCrO_3$ is a p-type conductor and shows a low electrical conductivity of ca. 0.6 $S \cdot cm^{-1}$ at 1000°C in air. Alkaline earth ion (Mg, Sr, and Ca) doping enhances the electrical conductivity by two orders of magnitude. Under hydrogen, Sr-doped $LaCrO_3$ exhibits the highest conductivity (4). The conduction mechanism of

[1] To whom correspondence should be addressed. Fax: (33) 04 76 82 66 70. E-mail: alsauvet@hotmail.com.

0021-9517/02 $35.00

doped lanthanum chromites is relatively well established. At high P_{O2}, the substitution of a trivalent ion by a divalent one is electronically compensated for by the formation of chromium ions in the formal +IV oxidation state. The oxygen deviation from stoichiometry (δ) is close to zero. At low P_{O2}, δ increases and oxygen vacancies are formed. Charge neutrality is maintained by reduction of Cr(IV) to Cr(III) (5, 6). Moreover, $La_{1-x}Sr_xCrO_3$ is mechanically and chemically stable under reducing atmosphere during a period of 1000 h (7). Vernoux (8) has shown that strontium-doped lanthanum chromites present interesting activity for hydrogen electrochemical oxidation but do not catalyze methane reforming (9).

Some metals (Pt, Rh, Ru) are known to exhibit high activity for methane steam reforming. Suzuki *et al.* (10) have tested Ru/ZrO_2 and Ru/Al_2O_3 cermets under SOFC anode operational conditions. Ru metal has high steam reforming reaction activity, carbon deposition resistance, and sintering resistance. Vernoux *et al.* (11) reached the same conclusion. However, cost and evaporation above 1200°C to form RuO_4 impede the use of ruthenium as a SOFC anode material.

The aim of this paper is to characterize anode materials obtained by insertion of ruthenium into $La_{1-x}Sr_xCrO_3$ to stabilize the ruthenium ion. We have synthesized the tested powders by the pyrosol technique (12). The catalytic activity was determined with a test rig using gas chromatography as analyzing device (13). The highest steam reforming efficiency was observed with 5% of ruthenium above 750°C for a steam/methane ratio equal to 0.175. No carbon deposition was detected and the catalytic activity was stable for more than 200 h under reducing conditions.

The stabilization of the ruthenium ion in the perovskite powder under reducing conditions at high temperature was evidenced by various analysis techniques.

2. EXPERIMENTALS METHODS

2.1. Catalyst Preparation

Table 1 gives the list of the investigated materials. The particle sizes were measured by laser granulometry and the specific area by the Brunauer–Emmett–Teller (BET) method with nitrogen at 77 K. The powders were prepared by the spray-pyrolysis technique (12) using an ultrasonic atomizer. The precursor solution consisted of lanthanum, chromium, strontium, and ruthenium nitrates in stoichiometric ratio. The final solution concentration was 5×10^{-2} mol · L^{-1}. The aqueous solution was atomized by a high-frequency (1.7 MHz) ultrasonic mist generator with piezoelectric ceramic transducers. The gas ($N_2 + O_2$ mixture) carried the aerosol with a flow rate of 6 L · min^{-1} through a tubular furnace heated at 800°C.

After synthesis, the powder was sintered at 1100°C for 1 h in air to complete the solid-state reaction. The results of the chemical analyses (realized in the CNRS Central Analysis Service, Vernaison) are summarized in Table 1. To quantify the different elements, preliminary treatments were carried out: for the lanthanum, the chromium, and the strontium an attack in perchloronitride was realized; for the ruthenium a fusion in soda at 450°C was carried out. The analyses were made by inductive coupling plasma atomic emission spectroscopy (IC-PAES).

2.2. Characterization Techniques

X-ray diffraction (XRD) patterns of the powders and electrode deposits, sintered at 1100°C for 4 h in air, were recorded with a Siemens diffractometer using $\lambda_{K\alpha}(Cu) = 1.5406$ Å. The step scans were taken over the range 2θ angles from 20 to 80° with 0.04° steps.

TPR (temperature-programmed reduction) analyses were carried out on $LaCrO_3$ (LC), LS30, LS30R5, and LS30R20. Each sample (100 mg) was placed on a fixed quartz bed in a reactor and flushed with helium gas (20 ml (STP) min^{-1}) for 15 min at room temperature. Then, the sample was pretreated in oxygen (20 ml (STP) min^{-1}) from room temperature to 600°C at a heating rate of 5°C · min^{-1}. Afterward, the sample was cooled to room temperature in the same atmosphere and the reactor purged by pure He for 15 min. A 1% H_2/He gas mixture (30 ml (STP) min^{-1}) was passed through the sample heated from room temperature to 900°C at a constant rate of 20°C · min^{-1}, followed by a plateau of ca. 30 min at 900°C. The species followed were

TABLE 1

Investigated Materials and Results of Chemical Analyses

Sample	Symbols	%wt La	%wt Sr	%wt Cr	%wt Ru	Calculated formula by assuming O_3[a]
$La_{0.8}Sr_{0.2}Cr_{0.95}Ru_{0.05}O_3$	LS20R5	49.15	7.10	20.74	2.49	$La_{0.81}Sr_{0.19}Cr_{0.942}Ru_{0.058}O_3$
$La_{0.7}Sr_{0.3}Cr_{0.95}Ru_{0.05}O_3$ (1st synthesis)	LS30R5	43.90	10.69	21.07	2.44	$La_{0.72}Sr_{0.28}Cr_{0.945}Ru_{0.055}O_3$
$La_{0.7}Sr_{0.3}Cr_{0.95}Ru_{0.05}O_3$ (2nd synthesis)	LS30R5	43.58	10.85	19.90	2.32	$La_{0.72}Sr_{0.28}Cr_{0.944}Ru_{0.056}O_3$
$La_{0.7}Sr_{0.3}Cr_{0.8}Ru_{0.2}O_3$	LS30R20	42.51	10.38	17.08	7.20	$La_{0.72}Sr_{0.28}Cr_{0.82}Ru_{0.18}O_3$
$La_{0.6}Sr_{0.4}Cr_{0.95}Ru_{0.05}O_3$	LS40R5	38.46	14.70	21.62	2.51	$La_{0.62}Sr_{0.38}Cr_{0.944}Ru_{0.056}O_3$

[a] O was not analyzed.

H_2, CH_4, H_2O, N_2 or CO, O_2, and CO_2 ($m/e = 2, 15, 18, 28, 32$, and 44 uma, respectively). For the TPD (temperature-programmed desorption) experiment, the same procedure was employed, but a pure He stream was used instead of 1% H_2/He.

EDX analyses were carried out on the LS30R5 and LS30R20 samples. The powders were milled and coated in organic resin. The resin was cut up in fine slices of 80 nm. The slices were deposited on a grid to analyze 200-nm zones. Transmission electronic microscopy (TEM) and energy-dispersive X-ray (EDX) analyses were carried out.

Thermogravimetric analyses (ATG) of LS30R5 were performed by placing 60 mg of a powder in a platinum crucible and increasing the temperature in a 5% H_2/Ar gas mixture from room temperature to 950°C at a constant rate of $4°C \cdot min^{-1}$.

Photoelectron spectra (XPS) were measured with a XR3E2 model vacuum generator. The LS30R5 and LS40R5 powders were mixed with YSZ powder at a 75/25 volume ratio to improve the adherence of the deposit on the YSZ pellet. Anode slurries, made by adding ethanol, polyvinyl butyral, polyvinyl pyrrolidone, and terpineol, were pulverized by spray on an 8YSZ plate, 1.5 mm thick and 18 mm in diameter. All the deposits were sintered at 1100°C for 4 h in air. Before recording the spectra, the pellet was sintered under different conditions, summarized in Table 2. LS30R5-ref is a pellet only sintered at 1100°C for 4 h in air, without treatment in reducing atmosphere. All binding energies were referred to the C 1s line at 285 eV.

Microprobe analyses were carried out on LS30R5-ref, LS30R5-H_2, and LS30R5-CH_4. The samples were covered by organic resin and polished until mirror face. We measured the ruthenium content within the electrode thickness, near the surface, in the middle of the deposit, and near the electrolyte surface.

2.3. Catalytic Activity

The catalytic activities of these powders were evaluated by analyzing the products by gas chromatography. The vector gas used was helium; the operating temperature was between 750 and 850°C. The methane content and the steam content were, respectively, changed between 5 and 30% for methane, 1.5 and 3.5% for steam. The experimental setup was described in more detail in (13). Steam was the minor reactive. To describe the activity, three parameters were used: the steam conversion (Eq. 5), the methane conversion (Eq. 6), and the carbon monoxide selectivity (Eq. 7).

TABLE 2

Preliminary Treatments of Samples Studied by XPS

Sample	Preliminary treatments	Symbol
LS30R5	Sintered at 1100°C 4 h in air	LS30R5-ref
LS30R5	Sintered at 1100°C 4 h in air and treated at 850°C, under H_2 for 15 h	LS30R5-H_2
LS30R5	Sintered at 1100°C 4 h in air and treated at 850°C, under CH_4 for 15 h	LS30R5-CH_4
LS40R5	Sintered at 1100°C 4 h in air and treated at 850°C, under H_2 for 15 h	LS40R5-H_2
LS40R5	Sintered at 1100°C 4 h in air and treated at 850°C, under CH_4 for 15 h	LS40R5-CH_4

$$C_{H_2O} = 100 \times \left(1 - \frac{P_{(H_2O)_f}}{P_{(H_2O)_i}}\right), \quad [5]$$

where $P_{(H2O)_i}$ is the initial steam pressure and $P_{(H2O)_f}$ is the final steam pressure.

$$C_{CH_4} = 100 \times \left(1 - \frac{P_{(CH_4)_f}}{P_{(CH_4)_i}}\right), \quad [6]$$

where $P_{(CH4)_i}$ is the initial methane pressure and $P_{(CH4)_f}$ is the final methane pressure.

$$S_{CO} = 100 \times \left(\frac{P_{CO}}{P_{CO} + P_{CO_2}}\right), \quad [7]$$

where P_{CO} is the final carbon monoxide pressure and P_{CO2} is the final carbon dioxide pressure.

3. RESULTS AND DISCUSSION

3.1. Chemical Analysis

As seen in Table 1, the powders compositions matched the desired stoichiometry. No loss of ruthenium was observed even after sintering in air at 1100°C and under catalytic activity measurement condition, i.e., under more than 200 h in methane at 850°C.

The specific area was 2 $m^2 \cdot g^{-1}$ for all these powders. From this result, we have calculated the grain size. The density of these powders was measured by a picometer and was around 3.8 $g \cdot cm^{-3}$. Assuming a spherical geometry ($R = \frac{3}{d \times S}$, with R the grain radius, d the powder density, and S the specific area), we obtained 0.3 μm as grain radius. In the case of cylindrical geometry ($R = \frac{2}{d \times S}$), the grain radius was 0.25 μm. In summary, the grain size was around 0.5–0.6 μm.

3.2. X-Ray Diffraction

In Fig. 1 are compared the X-ray diffraction patterns of LS30, LS20R5, LS30R5, and LS40R5 powders, sintered 1 h at 1100°C in air. No intermediate phase containing ruthenium was detected. An intermediate phase, $SrCrO_4$, was detected around 25–30°. However, as shown in Fig. 2, no intermediate phase was observed on the X-ray diffraction pattern of electrode deposits after sintering at 1100°C for 4 h in air. The additional peaks observed on the LS30R5 deposit spectra correspond to YSZ added in the ink to improve the adherence of the deposit on the YSZ pellet.

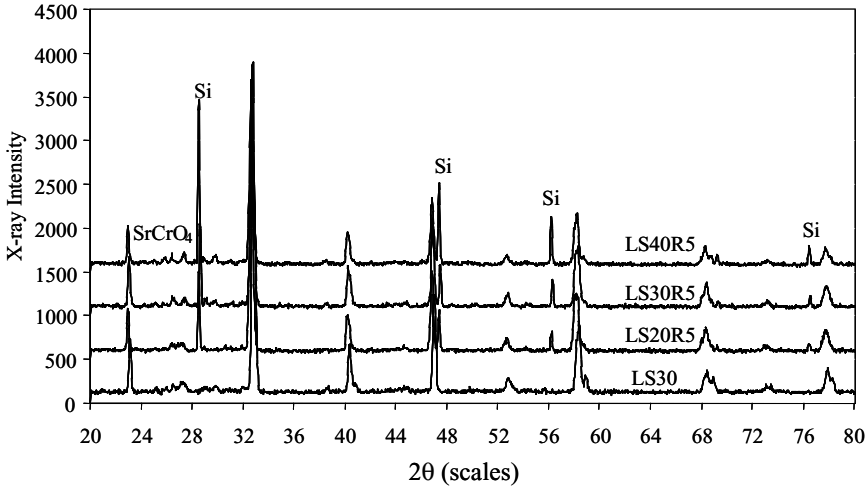

FIG. 1. X-ray diffraction patterns obtained for LS30, LS20R5, LS30R5, and LS40R5 powders.

Crystallographic parameters are summarized in Table 3; they are determined in a hexagonal unit cell with 0.025% error. The volume of a hexagonal system is $V = (\sqrt{3}/2)a^2c$. X-ray indexes verify the following relation: $-h + k + l = 3n$. The system has not a hexagonal unit cell but a rhomboedric one. Ruthenium substitution increases the volume. However, with regard to X-ray spectra (few rays and sweeping only to 80°), complementary studies should be carried out to determine the limit of ruthenium insertion and the possible modification of the crystallographic parameters. The crystallite size was calculated by the half-width and was ca. 30 nm.

3.3. Catalytic Activity

We observed that LS20R5 and LS30R5 have very similar catalytic activities. Vernoux (9) has studied the catalytic activity of $LaCr_{0.95}Ru_{0.05}$ at 800°C under a steam/methane ratio equal to 0.75. The initial activity of this powder was low and increased until 100% of steam conversion after 40 h of analysis. This behavior was explained by a progressive and reversible reduction of the ruthenium in the perovskite. In our studies, the steam conversion with LS20R5 or LS30R5 was immediately equal to 100% for the whole ratio range studied, i.e., 0.07 and 0.7, and this reaction was limited by steam content. We have not observed an increase in the catalytic activity. So, the strontium doping seems to influence the ruthenium stability in the perovskite and also the catalytic activity. However, we have observed no difference between LS20R5 activity and LS30R5 activity. We obtained 100% steam conversion down to 750°C.

In all the cases, no carbon deposition was detected and no degradation of the catalytic activity was observed after more than 200 h under operating conditions.

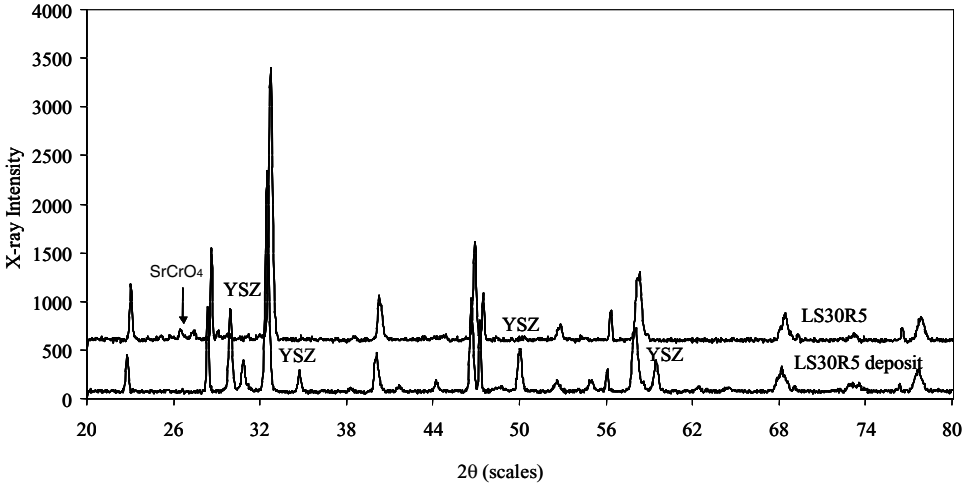

FIG. 2. X-ray diffraction patterns obtained for LS30R5 powder and LS30R5 deposit.

TABLE 3

Calculated Crystallographic Parameters of the Studied Samples in the Hexagonal System

Sample	a (Å)	b (Å)	c (Å)	Volume (Å^3)
$La_{0.75}Sr_{0.25}CrO_3$, data JCPDS	5.403	5.403	13.301	336.27
LS20R5	5.507	5.507	13.562	356.19
LS30R5	5.494	5.494	13.438	351.27
LS30R20	5.500	5.500	13.425	351.70
LS40R5	5.496	5.496	13.330	348.70

3.4. Scanning Electronic Microscopy Analysis (SEM)

No significant difference was observed as a function of the strontium content. The grain size was around 0.2–0.5 μm, with a few 1-μm agglomerates. These results agree with the grain size measured from the specific area.

As shown in Fig. 3 (EDX cartography), all the elements are homogeneously distributed. No segregation of ruthenium was observed.

3.5. Temperature-Programmed Reduction (TPR)

Figure 4 shows the TPR spectra run on for samples LC, LS30, LS30R5, and LS30R20 under 1% H_2/He. In the range 25–400°C, no chemical reduction was detected. Undoped sample (LC) revealed a weak reduction peak at 530°C. Strontium-doped samples had a large reduction peak which started at 550°C and which was incomplete at 900°C. With ruthenium-doped samples, a shift of the peak toward lower temperatures was observed. The hydrogen quantities consumed at ambient temperature and during the reduction treatment at 900°C are given in Table 4.

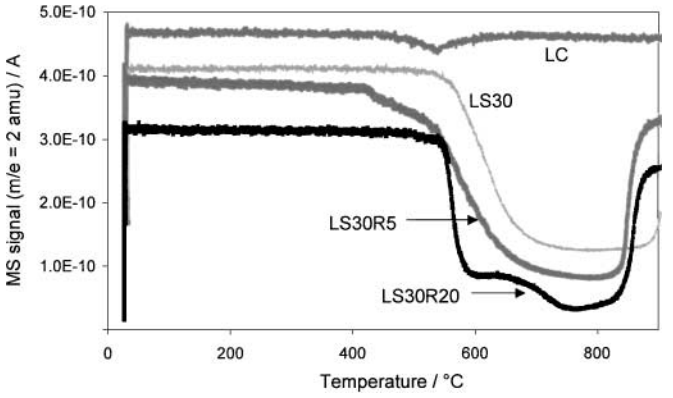

FIG. 4. TPR spectra of LC, LS30, LS30R5, and LS30R20. Profile of signal at $m/e = 2$ amu.

Compared to the results obtained for LC, it seems that the hydrogen quantity consumed for the reduction of strontium-doped samples cannot be explained by the reduction of Cr(III) to Cr(II). Moreover, ruthenium has no influence on the hydrogen quantity necessary for the reduction. The quantity of hydrogen consumed was close to the strontium content (Tables 4 and 5). The difference observed between the hydrogen quantity consumed and the strontium micromole quantity results probably from the secondary-phase $SrCrO_4$, observed on RX spectra realized with these powders sintered at 1100°C during 1 h in air.

As the reduction peak was not observed with LC powder, it could be related to strontium. This peak could be ascribed to the reduction of Cr(IV), which is produced to compensate electronically for the substitution of a trivalent ion La(III) with a divalent Sr(II) according to the

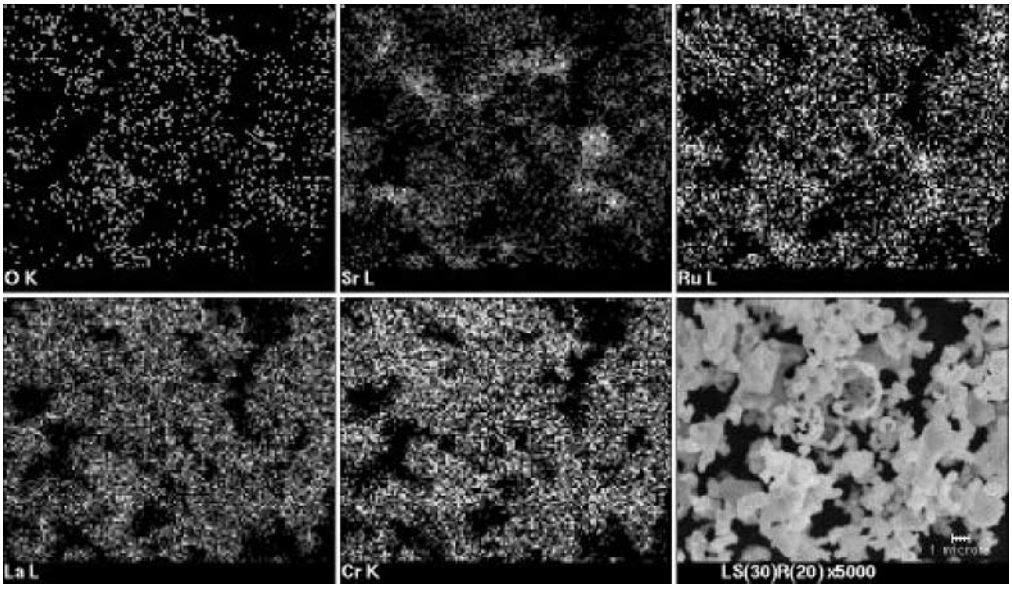

FIG. 3. EDX cartography of LS30R20.

TABLE 4

TPR Quantitative Analyses

Sample	H_2 consumed at 25°C (μmol $H_2 \cdot g^{-1}$)	H_2 consumed during the reduction peak (μmol $H_2 \cdot g^{-1}$)
LC	3	25
LS30	Not detectable	1749
LS30R5	1	1619
LS30R20	97	1873

Kröger–Vink notation (14):

$$(1-x)LaO_{1.5} + xSrO + CrO_{1.5} = (1-x)La_{La}^{x} + xSr'_{La} + (1-x)Cr_{Cr}^{x} + xCr_{Cr}^{\bullet} + (3-0.5x)O_{O}^{x} + 0.5V_{O}^{x}. \quad [8]$$

Similar results have previously been described with strontium-substituted lanthanum manganites (15) and with calcium-substituted lanthanum chromites (16).

The ruthenium, Ru(IV), was substituted for Cr(IV). The reduction peak does not decrease as a function of ruthenium content.

$$(1-x)LaO_{1.5} + xSrO + (1-y)CrO_{1.5} + yRuO_2 = (1-x)La_{La}^{x} + xSr'_{La} + [1-(x+y)]Cr_{Cr}^{x} + xCr_{Cr}^{\bullet} + yRu_{Cr}^{\bullet} + [3-0.5(x-y)]O_{O}^{x} + 0.5(x-y)V_{O}^{x}. \quad [9]$$

Moreover, in comparing the chemical potential of Cr_2O_3/CrO_2 ($\mu^\circ = +10.575$ kJ) and Ru_2O_3/RuO_2 ($\mu^\circ = -56.304$ kJ) at 25°C, Cr(IV) would be reduced before Ru(IV).

The co-doping with Sr(II) is therefore compensated for by the formation of Cr(IV). The ruthenium(IV) is stabilized because the Cr(IV) is more easily reduced. This explanation only holds if the amount of hydrogen consumed is totally used to reduce Cr(IV) to Cr(III). More particularly, one can consider that some carbonate species are present in the bulk of the perovskite (or more likely on its surface) and may be thermally decomposed, leading to the evolution of CO_2. Carbon dioxide could then react with hydrogen present in the stream to form $CO + H_2O$ (reverse water–gas shift reaction) or $CH_4 + H_2O$ (methanation). The observation of profiles at $m/e = 15$ and 28 amu indicates that neither CH_4 nor CO evolution is detected within the temperature range where reduction occurs. The profiles reported in Fig. 5 are relative to signals at $m/e = 32$ and 44 amu (related to O_2 and CO_2, respectively), under TPR and TPD conditions, for a LS30R20 sample. TPD is realized under a stream of pure He. Under both TPR and TPD conditions, a peak related to CO_2 evolution is observed within the temperature range where reduction occurs. The CO_2 profiles are quite similar in H_2/He and in pure He. The quantities evolved are 5.6 and 6.5 μmol of CO_2/g, respectively. These amounts are very small and roughly correspond to the amount of Sr expected at the sample surface. The absence of methane production from CO_2 during TPR is consistent with the presence of nonmetallic ruthenium species. Like nickel-based ones (17), ruthenium-based catalysts may be used successfully for CO_2 methanation (18) but they necessitate Ru to be in the reduced state (19). Profiles at $m/e = 32$ amu are very different under TPR and TPD conditions. In the TPR experiment, no peak is detected. Conversely, under TPD conditions, a strong peak related to O_2 evolution is observed, for a temperature higher than 700°C or so. The amount of oxygen detected is 280 μmol

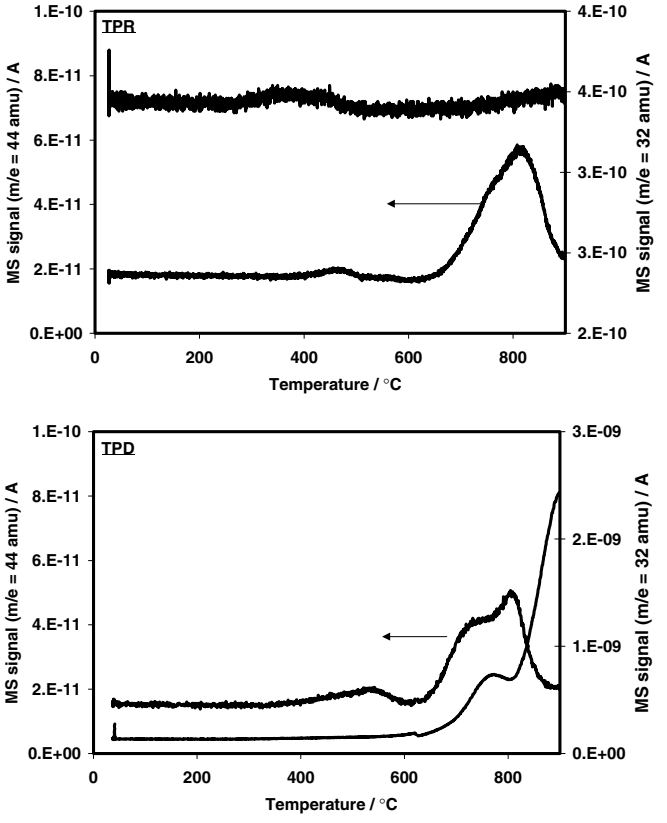

FIG. 5. TPD and TPR spectra of LS30R20. Profiles of signals at $m/e = 44$ and 32 amu.

TABLE 5

Compositions of the Samples Calculated from the Chemical Analysis, Except for LS30, Which Was the Theoretical Composition

Sample	La (μmol $\cdot$ g^{-1})	Sr (μmol $\cdot$ g^{-1})	Cr (μmol $\cdot$ g^{-1})	Ru (μmol $\cdot$ g^{-1})	M (g $\cdot$ mol^{-1})
LS30	3132	1342	4474	0	223.52
LS30R5	3168	1232	4153	246	227.29
LS30R20	3085	1200	3513	771	233.38

TABLE 6

Compositions (at%) of the Different Elements Detected by EDX for LS30R5

Area	Theor at% (zone)	O (60)	Cr (19)	Sr (6)	Ru (1)	La (14)
1	8	54.9	24.1	3.2	1.8	16
	9	59.9	21.7	2.8	1.4	14.2
	10	53.7	23.9	3.4	1.6	13.9
	11	60.2	21.8	2.7	1.3	16.0
	12	56.0	22.7	3.3	2.1	14.9
	13	59.9	20.4	3.3	1.5	11.0
	14	72.0	13.4	1.9	1.6	
2	15	58.7	22.1	3.2	1.2	14.7
	16	56.1	22.6	3.6	1.4	16.3
	17	59.6	20.5	2.9	1.6	15.4
	18	56.4	23.3	3.1	1.4	15.8
	19	60.1	20.6	2.4	1.2	15.7

of O_2/g and therefore would necessitate 560 μmol of H_2/g to be fully converted to H_2O, as suggested by profiles in TPR conditions. This quantity, not employed for Cr(IV) reduction into Cr(III), corresponds to the excess of hydrogen consumption observed when comparing data from Tables 4 and 5 (H_2 consumed during reduction peak with respect to Sr concentration).

3.6. TEM and EDX Experiments

The results obtained by EDX are summarized in Table 6 for LS30R5 and in Table 7 for LS30R20. The measured atomic compositions are similar to those expected, except for strontium. A deficit of strontium compared to the theoretical atomic percentage was obtained. The main point concerns the ruthenium content: no loss of ruthenium was observed even for LS30R20 even after calcination in air at 1100°C.

TABLE 7

Compositions (at%) of the Different Elements Detected by EDX for LS30R20

Area	Theor at% (zone)	O (60)	Cr (16)	Sr (6)	Ru (4)	La (14)
1	7	33.9	28.5	3.9	8.0	25.6
	8	46.9	25.1	3.1	4.7	20.2
	9	46.5	25.6	3.7	3.8	20.3
	10	53.3	25.6	4.3	1.9	16.9
	11	61.3	15.7	2.2	3.8	17.0
	12	31.3	35.2	4.8	3.9	24.7
	13	45.2	27.3	4.4	2.7	20.4
2	14	46.0	25.5	3.8	4.4	20.2
	15	55.4	24.8	2.7	1.3	15.9
	16	61.6	19.9	2.6	1.3	14.6
	17	53.4	18.0	5.3	7.1	16.2
	18	51.4	17.3	6.2	7.8	17.3
	19	53.8	19.1	4.3	6.5	16.3

3.7. XPS Experiments

In spite of the deposit characteristics, i.e., porous and not smooth, microprobe analysis revealed no ruthenium or strontium concentration gradient with LS30R5-H_2 and LS30R5-CH_4. The composition was homogeneous over the whole thickness of the deposit, around 40 μm. Complementary results have been obtained by XPS, which provide more surface-sensitive data (around 0.5–5 nm).

In Fig. 6 are represented the ratio between the atomic percentage determined for each element and the La + Sr + Cr + Ru sum. This representation allows one to eliminate the O 1s and C 1s participation and to highlight possible surface segregation. Several observations could be made.

- For LS30R5-ref, the ratios are similar to those obtained for the bulk.
- The treatments in reducing atmosphere (hydrogen or methane) modify the surface composition with a large decrease in lanthanum content and an increase in strontium content for LS30R5 and for LS40R5.
- The ratio (La + Sr)/sum is constant for all the samples, near the theoretical value of 0.5. The perovskite has the structure ABO_3. The increase in strontium content occurs to the detriment of lanthanum content, and the balance between elements on site A (La and Sr) and the elements on site B (Cr or Ru) is maintained.
- For elements on site B (Cr and Ru), treatment under hydrogen or under methane seems to favor a slight increase in ruthenium content and the concomitant decrease in chromium content.

The lanthanum spectra are similar to that measured for La_2O_3. Energy position of La $3d^{5/2}$ (834.8 eV) and spin-orbit splitting (16.8 eV) correspond exactly to that

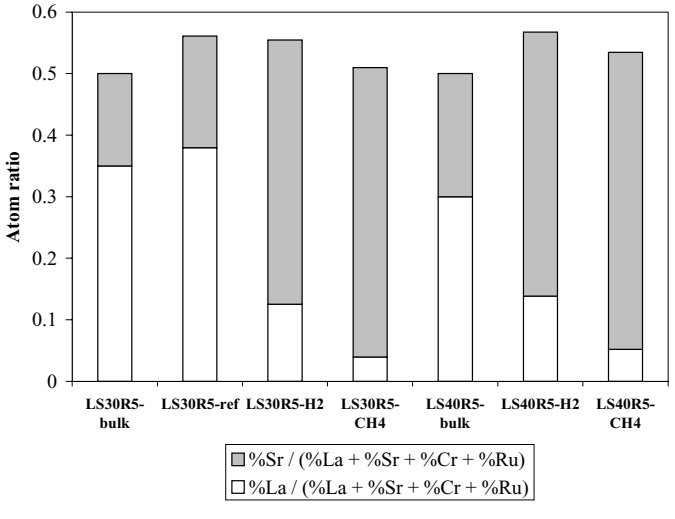

FIG. 6. Ratio between the atomic percentages of Sr and La and the sum (La + Sr + Cr + Ru) determined by XPS analyses.

of La_2O_3 (20). The different treatments do not modify form and position of peaks. The $3d^{5/2}$ and $3d^{3/2}$ strontium peaks obviously result from a mixture of at least two chemical species. As a function of the sample, peak maximum is between 134.5 and 135.2 eV, with no apparent relation to preliminary treatment. In the literature, we find 134.4 eV for Sr and 135.3 eV for SrO (21) but we have also to consider species such as strontium carbonates. For chromium, we observed essentially a Cr $2p^{3/2}$ peak maximum at 576.5 eV, corresponding to Cr(III) (22, 23). The spectrum of LS30R5-ref exhibits two weak peaks, at 580.1 and 589.7 eV. They can be attributed to the presence of Cr(VI), as reported by some authors for $La_{1-x}Sr_xCrO_3$ compounds obtained by the sol–gel route (24). Chromium(VI) compounds are characterized by Cr $2p^{3/2}$ peaks ranging from 578.3 to 580.1 eV, according to the chemical form, i.e., CrO_3, CrO_4^{2-}, or $Cr_2O_7^{2-}$ (22, 25). No trace of Cr(VI) can be detected after treatment under hydrogen or methane. Moreover, on LS30R5-ref, it seems that the peak shape at the low binding energy side indicates the presence of Cr(IV) (26). The determination of the ruthenium chemical state by XPS is not easy, as the Ru $3d^{5/2}$ peaks for Ru(0) and Ru(IV) are very close and the spin-orbit splitting is the same (27, 28). Moreover, C 1s and Sr $3p^{1/2}$ peaks interfere with Ru $3d^{3/2}$ and $3d^{5/2}$, respectively.

Figure 7 shows the oxygen spectra for the different samples. For LS30R5-ref, oxygen in structure (529.9 eV) is essentially observed. This result is in agreement with values obtained for $LaMn_{1-x}Cu_xO_3$ (29), 529.4–529.8 eV, and for $La_{1-x}Sr_xMnO_3$ (20), 529.3–529.9 eV. After treatment under hydrogen or methane, other structures at higher binding energy appear. This phenomenon is independent of the gas nature (hydrogen or methane) and increases with strontium content. It seems to be correlated with oxygen species adsorption on oxygen vacancies, during transfer in air, after reducing treatments. As an example, Tejuca *et al.* (30) observed 533.2 eV for adsorbed water molecules and 531.1 eV for hydroxyl groups.

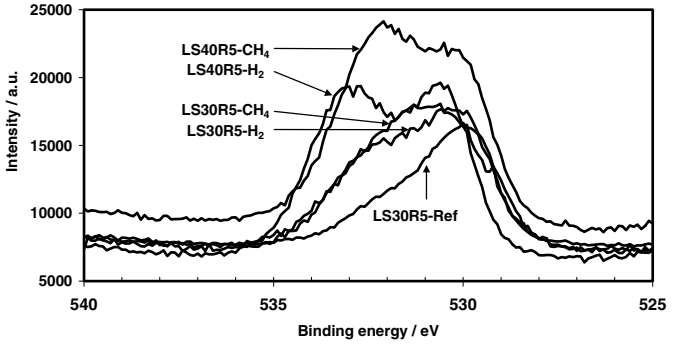

FIG. 7. Comparison of the oxygen XPS spectra obtained for the different samples.

3.8. Thermogravimetric Analyses (TGA)

Two plateaus were observed; the first weight loss began at 250°C and the second one at 800°C. This last temperature is 200°C higher than the beginning of hydrogen consumption observed by TPR. However, the temperature of the second TGA plateau corresponds to the beginning of water evolution, at about 750°C, observed during the TPR experiments. The temperature difference between the beginning of reduction and the beginning of water evolution (evidenced by both TGA and MS) precludes the possibility of a direct formation/desorption of water molecules. It is plausible that intermediate hydroxyl species (resulting from water dissociative adsorption) are formed after reduction of metallic ions, which leads to water desorption at higher temperatures, according to condensation of adjacent hydroxyl groups. The total mass loss was around 1.8 mg (3 wt%), corresponding to a deviation of the stoichiometry of 0.14. This mass loss is in good agreement with the mass of water, determined from the quantity of hydrogen consumed, evolved above 750°C during TPR experiment. Larsen *et al.* (31) have studied the conduction mechanism in $La_{1-x}Sr_xCr_{1-y}V_yO_{3-\delta}$ as a function of the oxygen pressure. At low P_{O2}, the oxygen loss is electronically compensated for by Cr(IV) reduction. These authors show that in considering the oxide chemical potentials and assuming that Cr(IV) and V(IV) are stabilized similarly in the perovskite lattice, the reduction of Cr(IV) is expected to occur at much higher P_{O2} than that of V(IV). In this case, δ increases with decreasing P_{O2} and reaches a saturation value equal to $(x - y)/2$ (see Eq. 9). If we calculate the saturation value of δ in our case, we obtain 0.125. This value is close to the experimental result ($\delta = 0.14$). This observation confirms that the ruthenium is in a tetravalent state.

3.9. Interpretation

The main use of ruthenium metal, in common with the other group VIII metals, is as a catalyst. In solution, ruthenium is employed in the tetravalent oxidation state (32–34), the most stable form of ionic ruthenium.

In reactions between a gas and a solid, for example in methane oxidation or methane reforming by carbon dioxide or steam, ruthenium is metallic and supported on SiO_2 or Al_2O_3. Matsui *et al.* (35) studied the reaction mechanism of carbon dioxide reforming of methane with Ru supported on La_2O_3, Y_2O_3, ZrO_2, and Al_2O_3. During the reaction, a part of metallic ruthenium reacted with CH_4 to give Ru–CH_x; simultaneously, ruthenium metal could be oxidized by CO_2 to give Ru–O_x and CO; then, oxygen transfer from Ru–O_x and Ru–CH_x took place to give CO and metallic ruthenium. The results of XRD analyses of Ru/La_2O_3 catalyst after CO_2 reforming exhibited diffraction peaks assignable to RuO_2 and Ru metal. Guerrero-Ruiz *et al.* (36) carried out isotopic experiments in syngas production from

methane on Ru/Al_2O_3 and Ru/SiO_2. They observed that an initial oxidation of the Ru surface would probably delay the formation of H_2 and CO. They also indicated that some authors propose that the most active form under dry reforming conditions was oxidized noble metal forms.

Several studies have shown the influence of the catalyst supports on the catalytic activity. As an example, Ferreira-Aparicio *et al.* (37) studied some mechanistic aspects of the dry methane reforming over Ru/SiO_2 and Ru/Al_2O_3. The support has great influence on the activity for dehydrogenation of methane and on the kind of carbonaceous species. With Ru/SiO_2, activation of both reactants takes place on the ruthenium surface. The accumulation of carbon adspecies formed from methane decomposition on the metallic particles finally impedes carbon dioxide dissociation and induces rapid deactivation of the catalyst. In contrast, with Ru/Al_2O_3, the alumina support participates in the activation of carbon dioxide by supplying hydroxyl groups (38, 39) according to

$$OH_{Al_2O_3} + Ru \rightarrow Ru\text{–}OH,$$

$$Ru\text{–}OH + Ru\text{–}C \rightarrow CO + \frac{1}{2}H_2 + Ru.$$

These authors proposed that the dry reforming of methane occurs through a Langmuir–Hinshelwood-type mechanism for Ru/SiO_2 in which both reactants are activated on the metallic phase. In contrast, a bifunctional mechanism, in which surface hydroxyl groups play a major role in the resistance to deactivation, is proposed for Ru/Al_2O_3.

Under our operating conditions of methane steam reforming, ruthenium is not metallic and not supported but is inserted as an ionic species into strontium-doped lanthanum chromites. The powder and deposit characterizations and the catalytic experiments have indicated the following:

- Metallic ruthenium is not detected even after reaction; TPR experiments allow detecting the presence of Cr(IV); ruthenium in tetravalent state would be substituted for Cr(IV); the quantity of hydrogen consumed during TPR was not related to the ruthenium content; Cr(IV) was more easily reduced than Ru(IV).
- Strontium is the key factor in explaining the stabilization of ionic ruthenium in the perovskite structure; Vernoux (9) observed a progressive and reversible reduction of ruthenium when $LaCr_{0.95}Ru_{0.05}O_3$ was used as a catalyst; the behavior difference can be explained only by the strontium doping.
- Strontium segregation was observed by XPS experiments; we observed also that, after treatment under reducing condition, other oxygen structures appear.

The catalytic activity of strontium- and ruthenium-doped lanthanum chromites could not be explained by the usual catalytic mechanism in which metallic ruthenium activates reactants.

Gellings and Bouwmeester (40), in a recent study of the solid-state aspects of oxidation catalysis, showed the influence of the solid-state effects on the catalytic activity. The main parameters of the catalytic activity are the following:

- nature of conduction (ionic, electronic or mixed)
- nature of the point defects
- interaction between defects
- oxygen vacancies formation in reducing atmosphere

In this connection, Driscoll *et al.* (41), who studied the methane oxidation on Li/MgO, showed that O^- ions at the surface activated methane reaction and reacted with Li^+ to form bidefects as $[Li^+O^-]$. In the same way, Steghuis *et al.* (42) observed that active sites for partial methane oxidation with TiO_2 are O^- at the surface of the catalyst. Saracco *et al.* (43) studied the methane decomposition with magnesium-doped lanthanum chromites. The magnesium present in the perovskite structure leads to a significant increase in the catalytic activity. They suggested that magnesium is located on the chromium sites of the perovskite according to Mg'_{Cr} which is accompanied by charge compensation, i.e., an increase in the charge of chromium, which are then present as $Cr^{\bullet}_{Cr}$. It is proposed that the increase in the catalytic activity can be explained by higher oxygen reactivity near the $Cr^{\bullet}_{Cr}$ defects.

In our study, strontium doping is compensated for by formation of $Cr^{\bullet}_{Cr}$. Under reducing conditions, oxygen vacancies are produced and Cr(IV) is reduced to Cr(III). On the surface of the catalyst, oxygen vacancy formation could be neutralized by strontium segregation within the subsurface. The oxygen vacancies could assist the steam dissociation in hydroxyl groups. Moreover, after reaction under methane, we have observed an increase in hydroxyl group concentration at the surface and a decrease in oxygen vacancies compared to the values obtained under hydrogen.

4. CONCLUSION

All the experimental results obtained by the different techniques indicate that the ruthenium ion is stabilized in the tetravalent state in the matrix. Moreover, the XPS analyses reveal that segregation of strontium occurs near the surface. This result is in agreement with the EDX analyses that indicate a concentration gradient of strontium within the subsurface. We cannot describe the different steps of the mechanism but some essential results were observed and they will allow optimization of new catalysts.

- Oxygen vacancies play a part in the catalytic mechanism.
- Strontium doping is compensated for by the formation of Cr(IV), and under reducing conditions, Cr(IV) is more easily reduced than Ru(IV); thus, the strontium doping

allows one to stabilize the ruthenium in the tetravalent state in the perovskite even during reaction processes.

• The activity of this catalyst for methane steam reforming in a methane-rich atmosphere (steam/methane ratio less than 1) is similar to that of ruthenium metal; however, we avoid ruthenium loss during preliminary treatment and the agglomeration of ruthenium particles during reaction.

REFERENCES

1. Ledjeff, K., Rohrbach, T., and Schaumberg, G., *in* "Proceedings of the 2nd International Symposium of SOFC's" (F. Grosz, P. Zegers, S. C. Singhal, and O. Yamamoto, Eds.), p. 323; Electrochemical Society, Pennington, NJ, 1991.
2. Vernoux, P., Guindet, J., and Kleitz, M., *J. Electrochem. Soc*. **145**, 3487 (1998).
3. Nakamura, T., Petzow, G., and Gauckler, L. J., *Mater. Res. Bull*. **14**, 649 (1979).
4. Mori, M., Yamamoto, T., Itoh, H., and Abe, T., *in* "Proceedings of the 2nd European SOFC Forum" (B. Thorstensen, Ed.), p. 465. Oslo, 1996.
5. Larsen, P. H., Hendriksen, P. V., and Mogensen, M., *J. Thermal Anal.* **49**, 1263 (1997).
6. Mizusaki, J., Yamauchi, S., Fueki, K., and Ishikawa, A., *Solid State Ionics* **12**, 119 (1984).
7. Milliken, C., Emangovan, S., and Khandler, A., *in* "Proceedings SOFC's III" (S. C. Singhal and H. Iwahara, Eds.), p. 335. Electrochemical Society, Pennington, NJ, 1993.
8. Vernoux, P., *Ionics* **3**, 270 (1997).
9. Vernoux, P., Thesis. INPG, Grenoble, 1998.
10. Suzuki, M., Sasaki, H., and Otoshi, S., *in* "Proceedings of the 2nd International Symposium of SOFC's" (F. Grosz, P. Zegers, S. C. Singhal, and O. Yamamoto, Eds.), p. 323; Electrochemical Society, Pennington, NJ, 1991.
11. Vernoux, P., Guindet, J., Gehain, E., and Kleitz, M., *in* "Proceedings of SOFC's V" (U. Stimming, S. C. Singhal, H. Tagawa, and W. Lehnert, Eds.), p. 219. Electrochemical Society, Pennington, NJ, 1997.
12. Djurado, E., Bouvier, P., and Lucazeau, G., *J. Solid State Chem*. **149**, 399 (2000).
13. Sauvet, A. L., and Fouletier, J., *J. Power Sources* **101**, 259 (2001).
14. Kröger, F. A., and Vink, H., *J. Solid State Phys*. **3**, 307 (1956).
15. Ponce, S., Peña, M. A., and Fierro, J. L. G., *Appl. Catal. B* **24**, 193 (2000).
16. Baker, R. T., and Metcalfe, I. S., *Appl. Catal. A* **126**, 297 (1995).
17. Twigg, M. V., "Catalyst Handbook," 2nd ed., Manson, London, 1996.
18. Fujita, S. I., and Takezawa, N., *Chem. Eng. J.* **68**, 63 (1997).
19. Gupta, N. M., and Kamble, V. S., *Indian J. Chem. Sect. A* **35**, 557 (1996).
20. Yong, W. Y., and Thorn, R. J., *J. Chem. Phys. Solids* **41**, 75 (1980).
21. Van Dovere, H., and Verhoeven, J. A., *J. Electron Spectrosc. Rel. Phenom*. **21**, 265 (1980).
22. Halada, G. P., and Clayton, C. R., *J. Electrochem. Soc.* **138**, 2921 (1991).
23. Battistoni, C., Dormann, J. L., Fiorani, D., Paparazzo, E., and Viticoli, S., *Solid State Commun*. **39**, 581 (1981).
24. Liu, X., Su, W., Lu, J., Pei, L., and He, L., *J. Alloys Compounds* **305**, 21 (2000).
25. Shuttleworth, D., *J. Phys. Chem*. **84**, 1629 (1980).
26. Cimino, A., De Angelis, A., Luchetti, A., and Minelli, G., *J. Catal*. **45**, 316 (1976).
27. Nyholm, R., and Martensson, N., *Solid State Commun.* **40**, 311 (1981).
28. Kim, Y. J., Gao, Y., and Chambers, S. A., *Appl. Surf. Sci.* **120**, 250 (1997).
29. Tabata, K., Hirano, Y., and Suzuki, E., *Appl. Catal. A* **170**, 245 (1998).
30. Tejuca, L. G., Bell, A. T., Fierro, J. L. G., and Penã, M. A., *Appl. Surf. Sci*. **31**, 301 (1998).
31. Larsen, P. H., Hendriksen, P. V., and Mogensen, M., *J. Therm. Anal.* **49**, 1263 (1997).
32. Caron, V., Thesis. INPG, Grenoble, 2000.
33. Ungermann, C., Landis, V., Moya, S. A., Cohen, H., Walker, H., Pearson, R. G., Rinker, R. G., and Ford, P. C., *J. Am. Chem. Soc.* **101**, 5922 (1979).
34. Atwood, D. K., and De Vries, T., *J. Am. Chem. Soc*. **84**, 2659 (1962).
35. Matsui, N., Anzai, K., Akamatsu, N., Nakagawa, K., Ikenaga, N., and Suzuki, T., *Appl. Catal. A* **179**, 247 (1999).
36. Guerrero-Ruiz, A., Ferreira-Aparicio, P., Bachiller-Baeza, M. B., and Rodriguez-Ramos, I., *Catal. Today* **46**, 99 (1998).
37. Ferreira-Aparicio, P., Rodriguez-Ramos, I., Anderson, J. A., and Guerrero-Ruiz, A., *Appl. Catal. A* **202**, 183 (2000).
38. Schuurman, Y., Marquez-Alvarez, C., Kroll, V. C. H., and Mirodatos, C., *Catal. Today* **46**, 185 (1998).
39. Ferreira-Aparicio, P., Rodriguez-Ramos, I., and Guerrero-Ruiz, A., *Appl. Catal. A* **148**, 343 (1997).
40. Gellings, P. J., and Bouwmeester, H. J. M., *Catal. Today* **58**, 1 (2000).
41. Driscoll, J., Martir, W., Wang, J.-X., and Lunsford, J. H., *J. Am. Chem. Soc*. **107**, 58 (1985).
42. Steghuis, G., Van Ommen, J. G., and Lercher, J. A., *Stud. Surf. Sci. Catal*. **119**, 831 (1998).
43. Saracco, G., Scibilia, G., Iannibello, A., and Baldi, G., *Appl. Catal. B* **8**, 229 (1996).